NUCLEAR TECHNOLOGY · VOLUME 211 · 2870–2879 · NOVEMBER 2025

DOI: https://doi.org/10.1080/00295450.2025.2461428

Note

An Anisotropic Neutron Collimating System for Proton Accelerator–Generated Secondary Particles

Brunilda Muçogllava,[a]* Selcen U. Duran,[a,b] and M. Bilge Demirköz[a]

[a]*Middle East Technical University, The Research and Application Center for Space and Accelerator Technologies (IVME-R), Ankara 06800, Turkey*
[b]*Karadeniz Technical University, Vocational School of Health Sciences, Trabzon 61080, Turkey*

Received May 31, 2024
Accepted for Publication January 12, 2025

Abstract — *Proton–stainless steel interactions occurring at the first collimator of the Middle East Technical University Defocusing Beamline generate high-energy secondary particles like neutrons (≤ 23 MeV), gamma rays (≤ 14 MeV), and electrons and positrons (≤ 7.0 MeV) with particle fluxes between 10^7 to 10^9 particles/(cm^2·s). A neutron collimating system aiming to reduce most of these secondaries and obtain a moderate flux of fast neutrons was designed and constructed. The collimating structure consists of a moderating unit aiming to shield the outside of the system, a neutron funnel to redirect the neutrons to the desired beam geometry, and a testing station. This system funnels neutrons into a 10-cm-diameter nonuniform beam and directs them to a testing area capable of hosting up to six samples of 7.3-cm diameter and up to 3.0-cm thickness. Simulation results show neutrons with energies up to 5.0 MeV and a flux of 10^6 neutrons/(cm^2·s) at the testing unit, while the experimental result gives a neutron dose rate of about 22 mSv/h.*

Keywords — *Neutron collimator, radiation testing, proton beamline, low-energy neutrons.*

Note — *Some figures may be in color only in the electronic version.*

I. INTRODUCTION

The study of neutron-matter interactions dates back to the discovery of the neutron particle and its neutral nature.[1] These interactions are primarily governed by short-range attractive nuclear forces and can be broadly categorized into two main processes: scattering and absorption.[2] Over time, these processes have led to the development of various applications, including neutron radiotherapy, nondestructive radiography, three-dimensional imaging, and material structure studies, among others.[3,4] To test neutron-matter interactions, low-flux neutron-emitting mixed-material matrices such as ^{239}Pu-Be and ^{241}Am-Be[5,6] or high-flux, high-energy nuclear fusion systems[6] are commonly used. This paper explores an alternative approach that involves a moderate flux and moderate-energy neutron testing station that utilizes secondary neutrons from a proton accelerator.

The Middle East Technical University (METU) Defocusing Beamline (DBL) is a proton beamline designed and constructed by The Research and Application Center for Space and Accelerator Technologies (IVME-R) at the Turkish Energy Nuclear and Mineral Research Agency's (TENMAK) Proton Accelerator Facility (PAF).[7] Its purpose is to perform single event effect tests.[8] PAF utilizes an IBA

*E-mail: bmucogll@uni-mainz.de

Cyclon 30 accelerator capable of delivering protons with energies ranging from 15 to 30 MeV.[8] These protons are directed to the research and development (R&D) room of the facility using one dipole, four quadrupoles, and a five-port switching magnet.[8] The beam currents can be adjusted from 0.10 to 200 μA, while the optical beam flux ranges between ~3.00 × 10^8 and 10^{10} protons/(cm^2·s), which meets the European Space Agency European Space Components Coordination No. 25100 standard, "Single Event Effects Test Methods and Guidelines."[7] Figure 1 shows a top view of the beamline, as reconstructed in the FLUKA simulation software,[9] with each of the components indicated with numbers 1 to 8.

Upon exiting the five-port switching magnet through the leftmost port (indicated with 1), the proton beam passes through the first collimator (indicated with 3). This collimator, composed of Type 316 stainless steel (SS316), has an aperture of 1.00 × 1.00 cm^2,[10] and it stops about 10% of the incoming protons. At the nominal beam rating [with a flux of 3.00 × 10^8 protons/(cm^2·s)], this corresponds to a loss of 6.20 × 10^{10} protons/s, each of which interacts with the SS316 and produces secondaries consisting mainly of neutrons, photons, electrons, and positrons. To prevent the R&D room from being contaminated with these secondaries, a hexagonal shield was placed around it.[10] The remaining protons pass through and undergo the defocusing process by quadrupole magnets 4, 5, and 6 before traveling through a 1-m-long path and reaching the second collimator at the end of the beamline (indicated with 7). The second collimator provides a proton irradiation area of 21.55 × 15.40 cm^2.[7] Figure 2 shows the entire beamline setup as photographed before October 2021.

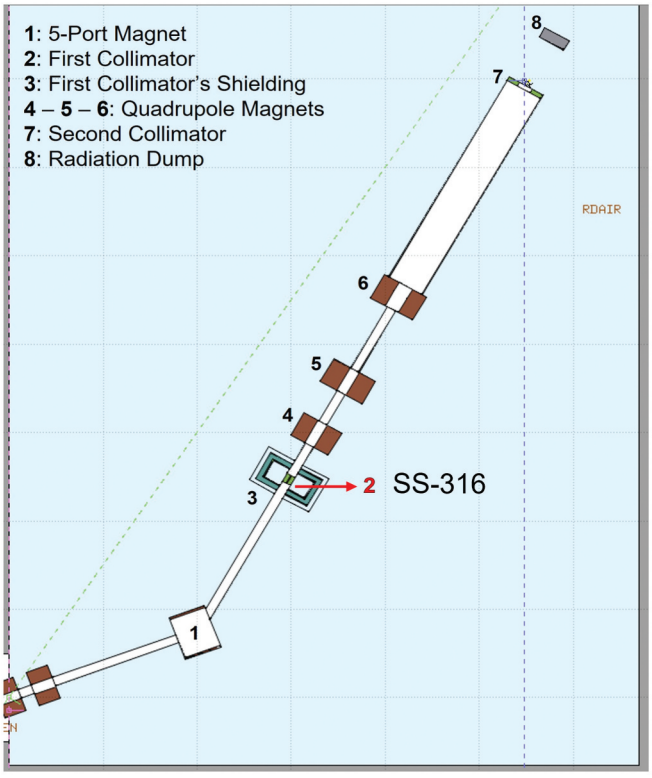

Fig. 1. The METU-DBL beamline structure as placed in the R&D room of TENMAK with its main components numbered 1 through 8 in the simulation program FLUKA.

Monte Carlo simulations of the secondaries produced at the first collimator indicated the presence of high-energy, high-flux neutrons resulting from the proton-SS316 interactions. As a response to this finding, a neutron collimating system was designed and constructed around the first collimator. The primary objective was to generate a neutron beam with a diameter of 10 cm and energies peaking at 5.00 MeV. The collimating system is intended to control and direct the neutron flux to achieve the desired beam characteristics.

Furthermore, a dedicated testing station was built to facilitate neutron-matter–interaction tests. This station offers a controlled environment where different materials and electronics can be placed and exposed to the neutron beam. The tests conducted at this station aim to study the effects of neutron irradiation on various materials and electronic components.[11,12]

II. METU-DBL COLLIMATOR SIMULATIONS

For this project, Monte Carlo simulations were conducted using FLUKA 4-1.1, a particle transportation and radiation-matter–interaction simulation tool[9] and Flair 3.1-15.1, a graphical user interface that facilitates geometry input and provides an interactive plotting Gnuplot-based tool.[13] For low-energy neutrons (with energies up to 20.0 MeV), the LOW-NEUT card with a multigroup transport module was utilized. Neutrons with energies above this threshold are automatically transported. The multigroup transport algorithm implements the MORSE Monte Carlo transport system, which assigns either 260 or 72 (optional) energy groups to the 0- to 20-MeV neutron energy interval and calculates group-to-group transfer probabilities for all scattering interactions. FLUKA's neutron cross-section library contains data for more than 250 materials, sourced from the ENEA-Bologna Nuclear Data Group, the Evaluated Nuclear Data File (ENDF), the Japanese Evaluated Nuclear Data Library (JENDL), and more. The full material table and the source library are available in the FLUKA manual.[14]

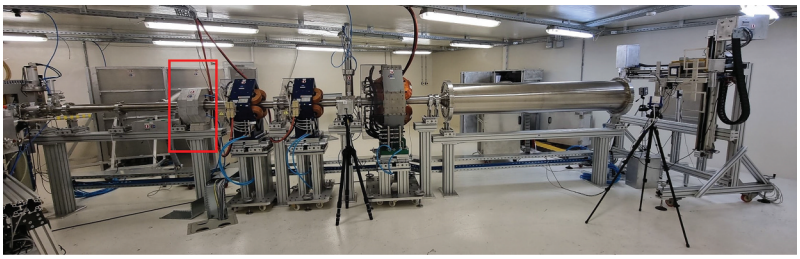

Fig. 2. The METU-DBL beamline setup, with incoming protons entering the pipeline from the left, through the first collimator indicated with a red box, and stopping at the test table or beam dump on the right.[10]

In this study, the simulations were carried out using 260 neutron energy groups, 42 gamma-ray production groups, default pointwise cross-section libraries, and default fission neutron multiplicity.[15] Each simulation consisted of 10 cycles with 2 million primary particles and a predefined initial seed for randomness in each run.

The Monte Carlo simulations were performed without including the shielding of the first collimator to assess the secondary particle production at this specific point. Additionally, an extra 1.00-cm-thick aluminum target was introduced in front of the beam dump at METU-DBL. The beam dump comprises a water-cooled 12.0-cm-thick block of 6082 aluminum alloy (Al 6082) covered with a 2.00-mm-thick graphite layer, designed to halt the proton beam from reaching the room's protective walls.[16] However, this setup generates a significant number of secondary particles, which are created and backscattered toward the first collimator. Consequently, this increases the number of recorded secondary particles in our region of interest. The inclusion of the aluminum target effectively reduces the production of secondary particles and introduces a larger scatter angle for the remaining ones. FLUKA scores particle fluence in particles/(cm^2·primary unit weight), where each produced primary has the same statistical weight. To obtain the beam flux, the simulation results are normalized by multiplying with the beam current. With our nominal beam parameters, for a 0.1-μ A proton beam, the normalization factor is calculated as 6.2×10^{18} protons/A $\cdot$ 0.1×10^{-6} A = 6.2×10^{11} protons.

The simulations result in a beam flux of $\sim 1.00 \times 10^8$ protons/(cm^2·s), which is consistent with the experimental measurements during beamline operation. Figure 3 displays the neutron flux distribution on the *X*-*Z* plane (top-down view), revealing two areas of interest: high neutron production from proton-SS316 interactions at the first collimator and proton–Al 6082 interactions at the target near the beam dump. Consequently, the first collimator emerges as the ideal setup location. However, it is essential to note that the neutron flux and energy range around the collimator vary significantly based on factors such as the distance from the beam, the angle, and the size of the scoring area. The ideal position for the neutron beamline, ensuring the achievement of the desired flux and energy, was determined to be at a 90-deg angle to the proton beam pipe, 127 cm from the floor, matching the height of METU-DBL. Precise alignment between the neutron and the proton beam centers is crucial to attain the maximum flux and energy of the produced secondaries.

While the flux can be further increased by intentionally shifting the proton beam away from its central position (on the horizontal axis only), which results in more protons being intercepted by the collimator, simulations and beam measurements demonstrate that this approach leads to the production of even higher-energy neutrons and gamma rays. The objective is to maintain a moderate flux and kinetic energy for the neutrons, so decentering the proton beam is discouraged. The desired balance between the neutron flux and energy for efficacious radiation testing can be achieved by adhering to the optimal alignment.

Table I provides details on the flux and kinetic energy range of the produced secondaries (neutrons, photons, and electron-positrons) scored at a 90-deg angle to the beam pipe, situated 1.00 cm from the collimator, with an effective scoring area of a 10-cm-diameter disk. These results show that the kinetic energy of neutrons can reach up to 23.0 MeV with a flux of approximately 2.30×10^8 neutrons/(cm^2·s), and the kinetic energy of photons can go up to 14.0 MeV with fluxes around 1.50×10^7 photons/(cm^2·s). Figure 4 shows the full kinetic energy spectrum of neutrons generated 1 cm from the first collimator. Each kinetic energy bin corresponds to one of the 260 neutron energy groups, with 31 bins representing the 0- to 0.5-MeV range.[14] The majority of the neutron flux is concentrated below 2 MeV, although the spectrum extends out to 23 MeV.

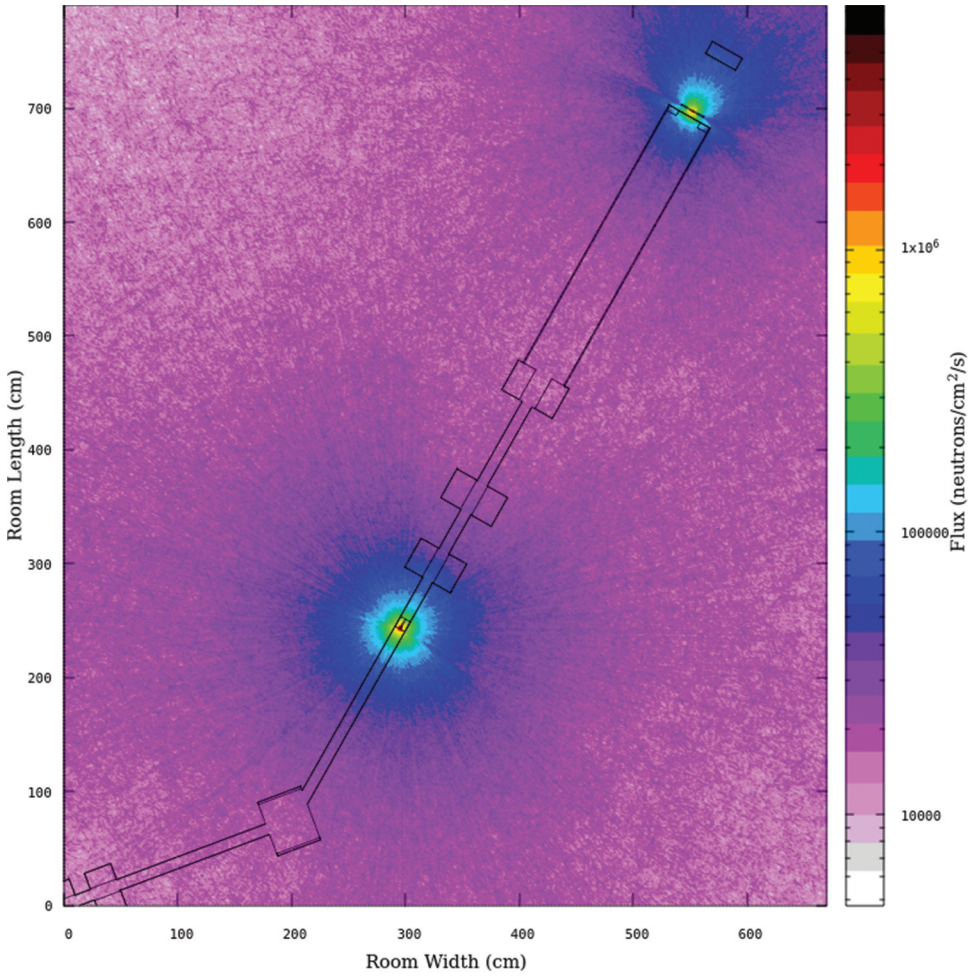

Fig. 3. The neutron flux [neutron/(cm^2·s)] distribution on the *X-Z* plane of the R&D room of METU-DBL as scored using FLUKA. Protons enter from the lower left, (0,0) coordinate and stop at (550,700), where a 1.0-cm-thick aluminum target is placed. Neutron production is observed mainly around the first collimator and the aluminum target.

Certain design choices for the neutron collimating system should be made to achieve the primary objective of a neutron beam with a diameter of 10 cm and energies of ~5.00 MeV. These requirements include a substantial reduction in the presence of photons, electrons, and positrons; the moderation of neutrons through scattering to lower energies suitable for radiation testing purposes; the efficient channeling of anisotropic neutrons into a well-defined neutron beam; reduction of secondary gamma rays from neutron-matter interactions; and the delivery of this beam to a designated test station. In light of these design goals, a formalized setup has been developed to achieve the desired outcomes.

TABLE I

Proton-SS316 Produced Secondary Particles and Their Corresponding Flux and Kinetic Energy Range*

	Flux [particle/(cm^2·s)]	Kinetic Energy Range (MeV)
Neutrons	$2.30 \pm 0.20 \times 10^8$	≤ 23.0
Photons	$1.50 \pm 0.20 \times 10^7$	≤ 14.0
Electrons-positrons	$1.20 \pm 0.10 \times 10^9$	≤ 7.00

*Scored with a detecting surface placed 1.0 cm (top) away from the beam pipe, aligned to the collimator's center at 90 deg to the proton beam.

III. DESIGN AND CONSTRUCTION

Figure 5 presents the finalized design of the neutron collimating system, comprising three main units denoted A, B, and C, all positioned at a 90-deg angle to the center of the collimator's aperture, situated 127 cm above the

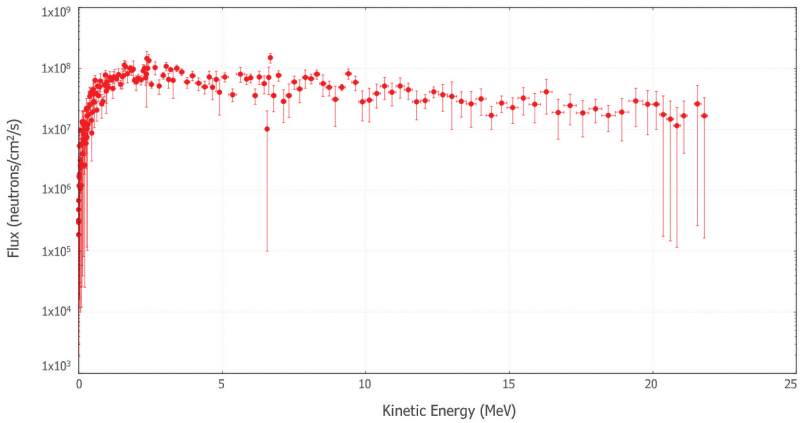

Fig. 4. The secondary neutron kinetic energy range 1 cm from the first collimator, extending to 23 MeV.

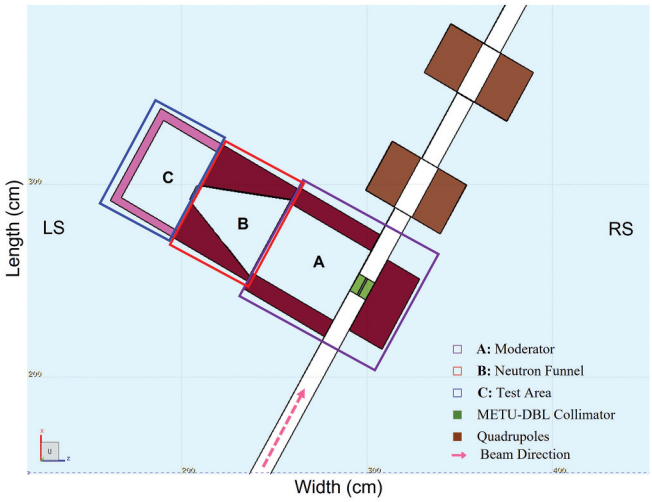

Fig. 5. The neutron collimating system's top view as seen in Flair and used in FLUKA simulations. Each of the three units, placed 90 deg to the beamline, are indicated with A, B, or C and respective colored boxes.

R&D room's floor. Unit A is designed to prevent radiation from escaping the station, thereby reducing room contamination and providing protection during beam-off work. The unit primarily consists of special-mix, high-density concrete blocks obtained from MODEDOOR, forming two side walls with a 9.50-cm thickness and a back wall measuring 19.0-cm thickness. Given its proximity to the room's exit door, the back wall has been reinforced with an additional 1.00-cm lead plate to enhance radiation shielding. For the top and bottom plates, a combination of Al 6082, high-density polyethylene (HDPE), and lead plates was utilized, offering effective radiation shielding without overburdening the unit with excessive weight. Table II provides more comprehensive details regarding the structure, dimensions, and materials used in all three units.

Unit B houses the primary collimating structure, featuring a neutron funnel. This funnel takes the form of a hollow rectangular prism, constructed from a composite, high-density concrete mixture, measuring 54.5 cm in height and width. Its interior is shaped as a truncated cone with a base diameter of 45.4 cm and a top diameter of 11.0 cm, and it is lined with paraffin. To create the funnel, a medium-density fiberboard (MDF) mold was utilized, which facilitated the pouring and shaping of the polyester mixture. Figure 6 illustrates the mold before construction (Fig. 6a) and the completed funnel (Fig. 6b). Initially, HDPE was considered as the neutron moderating material for the funnel; however, its size and shape necessitated specialized and large machinery, posing a high risk of machinery breakage during the fabrication process. Consequently, we opted for a polyester-based mixture after simulations demonstrated its suitability for use in a radioactive environment.

The chemical composition of the mixture is provided in Table III, as analyzed through X-ray fluorescence (XRF) spectroscopy. Simulations indicated that the material effectively prevented neutrons from escaping the defined region and significantly reduced the flux of other secondary particles. However, neutron-funnel interactions resulted in an increased gamma flux, leading to a relatively small neutron-to-gamma (n/γ) flux ratio at the funnel's exit. To address this, a 2.00-mm paraffin layer was introduced to the inner walls of the collimator, allowing for the reduction of produced gamma rays through dispersive refraction.[17] Prior to pouring the wax, the interior of the funnel was sanded using ISO P120 grit-sized sandpaper. The addition of paraffin effectively reduced the neutron collimator–produced gamma rays within the cone while also reducing the neutron flux inside the cone by approximately 10%. To further enhance the n/γ flux ratio, two lead plates, measuring 0.70 and 0.60 cm in thickness, respectively, were

TABLE II

Comprehensive Details Regarding the Structure, Dimensions, and Materials Used in Units A, B, and C*

Unit	Components	Material	Shape	Height (cm) × Width (cm)	Thickness (cm)
A	Side walls – left side (× 2)	High-density concrete	Wall	61.5 × 77.0	9.50
	Side walls – right side (× 2)	High-density concrete	Wall	81.5 × 59.5	9.50
	Back wall – 1	High-density concrete	Wall	80.5 × 45.0	19.0
	Back wall – 2	Lead	Slab	81.0 × 45.0	1.00
	Top plate – 1	HDPE	Slab	112 × 60.5	3.00
	Top plate – 2	Al 6082	Slab	112 × 50.0	0.50
	Bottom plate – 1	Lead	Slab	112 × 45.0	2.00
	Bottom plate – 2	Al 6082	Slab	112 × 80.0	1.00
	Gamma filter – 1	Lead	Slab	60.8 × 60.0	0.70
B	Funnel – outside	Composite[a]	Hallow rectangular prism	54.5 × 54.5	4.50 to 21.8
	Funnel – inside	Paraffin	Truncated cone	11.0 × 45.4[b]	0.20
	Gamma filter – 2	Lead	Slab	15.5 × 36.0	0.60
C	Side walls (×2)	HDPE	Wall	30.0 × 40.0	3.00
	Front wall	Paraffin	Block	—	1.00 to 3.00[c]

*The measurement station's structure is divided into three units: A, B, and C. The shapes, materials, sizes, and thicknesses of each component are given in the table.
[a]Funnel composition is given in Table III.
[b]Top and base diameter values.
[c]Several small uneven blocks of paraffin were used to build the front wall.

TABLE III

Chemical Composition of the Neutron Funnel*

Element	Mass (wt%)	Element	Mass (wt%)
Hydrogen	6.87	Silicon	1.38
Oxygen	54.1	Boron	1.27
Carbon	27.7	Magnesium	0.838
Calcium	13.9	Strontium	0.512

*Chemical composition is in units of weight percentage and analyzed using XRF spectroscopy at METU's Central Laboratory. Elements with weight percentage less than 0.1 have been ignored.

inserted at the base and top of the funnel to serve as gamma filters.

Unit C houses the testing station, which features the central rotating mechanism as its primary component. The design of this mechanism is given in Fig. 7a, while Fig. 7b provides details on its components, materials, and dimensions. The center of the mechanism consists of HDPE and contains six sample containers, each capable of holding samples with varying thicknesses ranging from 0.50 to 3.00 cm. These sample containers are positioned at the top of the funnel, centered to the neutron beam. To ensure accurate beam measurements and optimal proton beam alignment to the first collimator, the first sample holder remains empty.[15]

The upper back plate, indicated by 8, is removable, allowing for the placement of samples on the rotating disk. To measure the flux of neutron and gamma dose rates, a ^{3}He neutron detector (RadEye NL) and a beta-gamma dose rate Geiger-Mueller counter (J305) were placed behind the tested samples. The RadEye NL is a personal neutron detector with high neutron detection sensitivity and no gamma radiation spillover up to 10 mSv/h. The detector measures counts per second (cps) and converts them to μSv/h using an internal conversion parameter (0.3 cps = 1 μSv/h). This conversion parameter is derived from a ^{252}Cf calibration source, and the detector is used without any moderating material surrounding it. The Geiger-Mueller counter measures ionizing radiation and beta particles every 15s and multiplies the values by 4 to provide counts per minute (cpm), which are then converted to the ambient dose equivalent rate (123 cpm = 1 μSv/h).

Additionally, a camera was positioned on top of the system, providing a top-down view of the neutron

(a) (b)

Fig. 6. (a) The MDF mold used to shape the funnel to the desired geometry and dimensions and (b) the end product after the mixture had settled overnight.

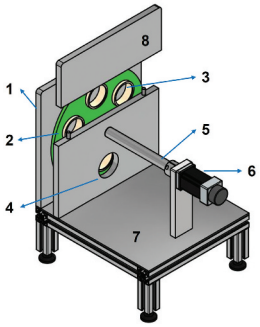

Identifiers	Component	Material	Height (cm) × Width (cm)	Thickness (cm)
1	Shielding Plate (×2)	Al-6061	40.0 × 40.0	2.0
2	Rotator	HDPE	36.0 [a]	1.0
3	Sample Holders	PLA	7.3 [b]	0.5
4	Radiation Path	Empty	7.8 [b]	2.0
5	Rotating Shaft	Al-6061	30.0 × 4.5 [c]	-
6	Servo Motor	-	16.5 × 6.0	-
7	Support Base	Al-6061	45.0 × 40.0	2.0

[a] disk diameter
[b] inner diameter
[c] length and diameter values

(a) (b)

Fig. 7. (a) The schematic drawing of the rotating mechanisms with numbers 1 through 7 denoting its different parts, with 8 denoting the removable upper plate, and (b) the corresponding geometries and materials used.

detector and the rotating mechanism's shaft, clearly indicating which sample is being tested at any given time. The rotation is driven by a servo motor, controlled remotely through a LabVIEW script[18] and a user interface, enabling control of the mechanism during the experiments. To safeguard the test station from external

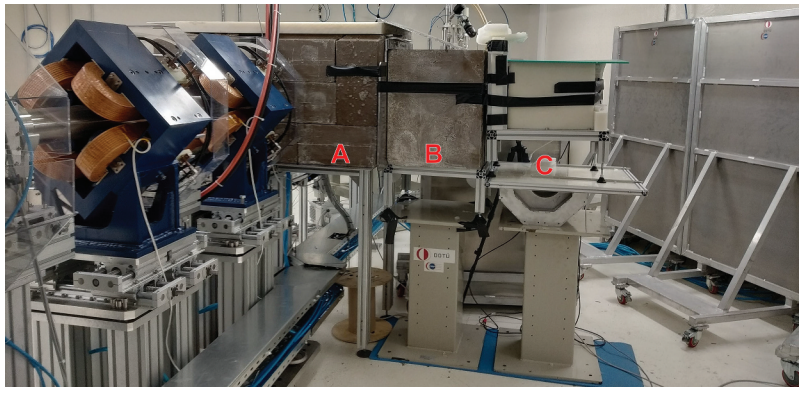

Fig. 8. The secondary measurement station as installed around the first collimator of METU-DBL.

radiation originating from the front of the proton beamline and the beam dump, the entire mechanism is covered using blocks of HDPE and paraffin, providing effective shielding. The final fully constructed system is depicted in Fig. 8, representing a complete and functional neutron collimating and testing setup.

IV. RESULTS

The system design was initially implemented in FLUKA, incorporating the specified dimensions from Table II. The detection area was defined as 7.30 cm in diameter and 2.0 cm in thickness to simulate possible sample geometries. Figure 9 gives the neutron flux distribution on the *Z-X* plane (top-down view) of the R&D room with the addition of the collimating system. When comparing with Fig. 3, it is evident that the neutron beam has been successfully collimated toward the intended testing station. In Table IV, the flux of secondary particles, along with their corresponding kinetic energy ranges, is presented scored at the exit of the neutron beam. The primary goal of achieving the desired neutron energy has been met. The directed neutron flux from the first collimator effectively reaches the test station while reducing the room's radiation dose, albeit with some loss in neutron flux. Furthermore, all electrons and positrons have been successfully stopped, and significant reductions in gamma radiation have been achieved.

Once the neutron station was constructed, several experimental runs took place. The neutron detector results in mSv/h are given in Fig. 10a, while the Geiger-Mueller counter beta-gamma ambient dose

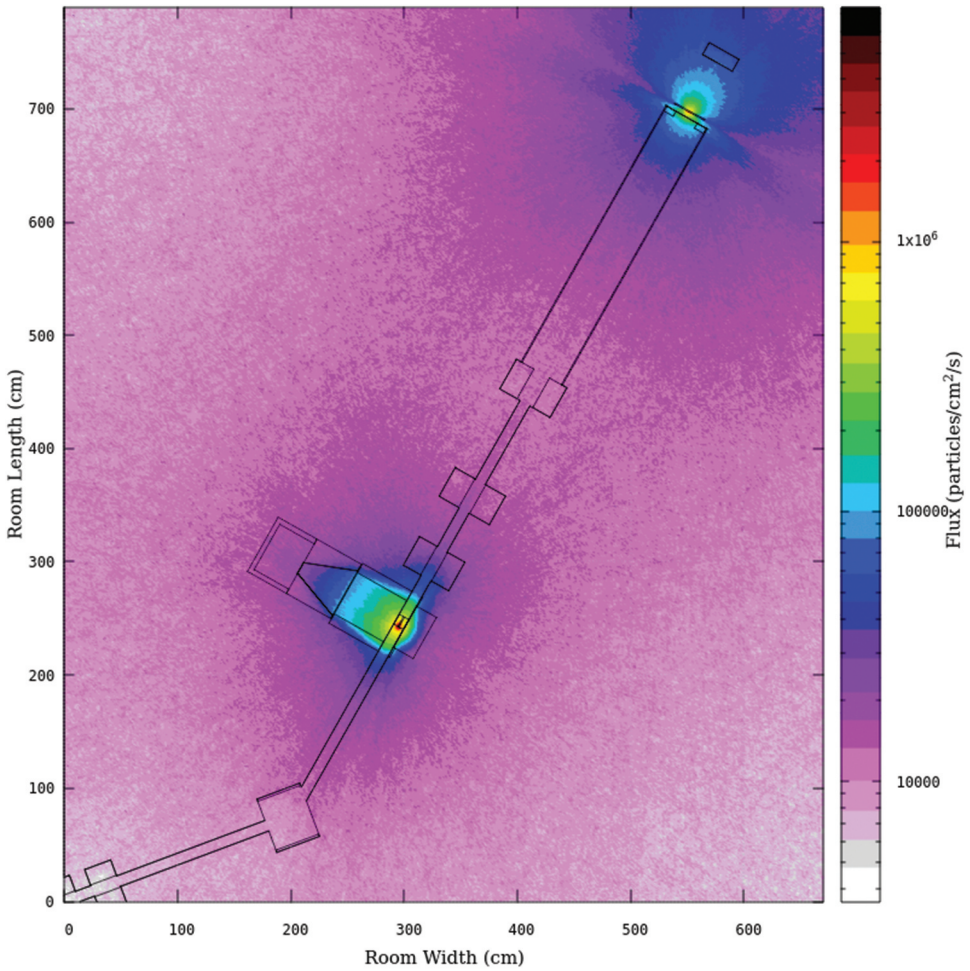

Fig. 9. The neutron flux [neutron/(cm^2·s)] in the R&D room of METU-DBL in the *Z-X* plane scored using FLUKA. Neutrons produced at the first collimator have been successfully moderated and funneled toward the test station using the neutron collimating system.

TABLE IV

Secondary Particles and Their Flux and Kinetic Energy Values at the End of the Neutron Funnel*

	Flux [particle/ (cm^2·s)]	Kinetic Energy Range (MeV)
Neutrons	$5.1 \pm 0.3 \times 10^6$	≤ 5.0
Photons	$7.7 \pm 0.8 \times 10^6$	≤ 4.5
Electrons-positrons	~ 0	~ 0.0

*Results obtained through FLUKA.

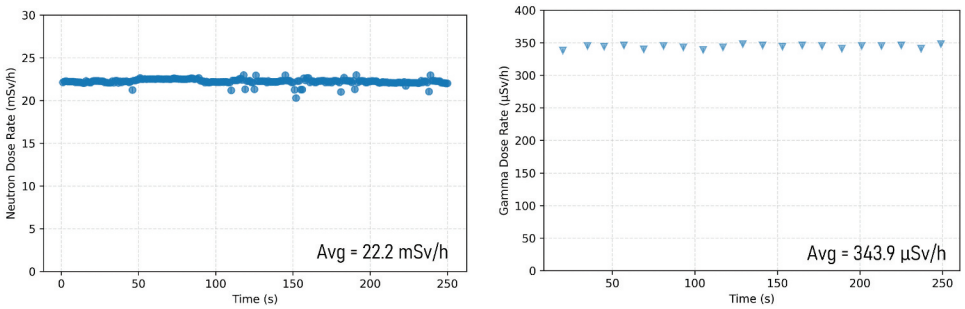

(a) (b)

Fig. 10. (a) The measured neutron dose rate (mSv/h) and (b) the gamma dose rate (μSv/h) during one of the first experimental runs using the new system.

rate results in μSv/h are presented in Fig. 10b as measured at the exit of the neutron beam. The measured neutron dose is significantly higher than the gamma dose. However, uncertainties associated with the conversion parameter of the neutron detector highlight the need for further calibration of the device, as well as a more precise estimation of measurement uncertainties, before a reliable neutron-to-gamma ratio can be determined. Further measurements using a BF_3 neutron counter will assist in accurately determining the neutron-to-gamma dose ratio of the testing station by providing more reliable neutron dose equivalent rate results. With the new detector, an improved method for flux and equivalent dose scoring in the FLUKA simulations will be introduced to enable an accurate comparison between the simulation results and the measurements carried out along the beamline.

Additionally, two Geiger-Mueller counters, one at the proton beamline's first collimator and the other at the R&D room's vault door, were used to monitor the ionizing radiation present in the room after the system's installation. For a typical run (0.1-μA proton beam current), the average gamma radiation dose rate at the first collimator was 1044 μSv/h while the average room dose rate was 94.7 μSv/h.

V. CONCLUSION

The experimental results obtained from the neutron collimating and testing setup at METU DBL have successfully achieved their design objectives. By effectively directing the neutron flux to the test station while significantly reducing the room radiation dose through the shielding and gamma-ray presence with the use of lead plates as gamma filters, the system has shown its proficiency in creating a neutron-rich environment. The experimental measurements align with the intended purpose, validating the setup's capabilities for radiation testing and material structure studies. Future work will focus on conducting experimental measurements of the neutron beams' kinetic energy range and testing a novel, layered, boron-based neutron shield.[15]

Overall, the neutron collimating system and the testing station represent essential additions to the facility, enhancing its capabilities for studying neutron interactions and enabling researchers to conduct comprehensive neutron irradiation experiments.

Acknowledgments

The authors extend their gratitude to TENMAK for its collaborative support and MODEDOOR for providing essential materials for the study.

Disclosure Statement

No potential conflict of interest was reported by the author(s).

Funding

This research was funded by the Scientific and Technological Research Council of Turkey under the grant (award number 5190039) and the Turkish Academy of Sciences and conducted at the METU in collaboration with The Research and Application Center for Space Accelerator Technologies, as well as with valuable contributions from the Karadeniz Technical University.

ORCID

Brunilda Muçogllava http://orcid.org/0000-0003-4212-7125

References

1. V. NESVIZHEVSKY and J. VILLAIN, "The Discovery of the Neutron and Its Consequences (1930-1940)," *C. R. Phys*., **18**, *9*, 592 (2017); https://doi.org/10.1016/j.crhy.2017.11.001.
2. I. OBODOVSKIY, "Chapter 7 – Interaction of Neutrons with Matter," *Radiation: Fundamentals, Applications, Risks, and Safety*, p. 151, Elsevier; https://doi.org/10.1016/B978-0-444-63979-0.00007-0.
3. E. B. PODGORŠAK, "Interactions of Neutrons with Matter," *Biological and Medical Physics, Biomedical Engineering*, p. 429, Springer; https://doi.org/10.1007/978-3-642-00875-7_9.
4. W. A. G. SAUERWEIN, "Principles and Roots of Neutron Capture Therapy," *Neutron Capture Therapy*, pp. 1–16, Springer, Berlin Heidelberg; https://doi.org/10.1007/978-3-642-31334-9_1.
5. ISO 14152:2001, *Neutron Radiation Protection Shielding—Design Principles and Considerations for the Choice of Appropriate Materials*, International Organization for Standardization (2001); https://www.iso.org/standard/33941.html.
6. S. N. AHMED, "Properties and Sources of Radiation," *Physics and Engineering of Radiation Detection*, 2nd ed., pp. 1–64, Elsevier; https://doi.org/10.1016/B978-0-12-801363-2.00001-2.
7. C. YAZGAN et al., "Performing the First Single Event Effect Tests Using the METU Defocusing Beam Line in Turkey," *RAD Associ. J.* **3**, 128 (2018); https://doi.org/10.21175/RADJ.2018.02.021.
8. M. DEMIRKOZ et al., "Metu-Defocusing Beamline: A 15-30 Mev Proton Irradiation Facility and Beam Measurement System," *EPJ Web. Conf*., **225**, 01008 (2020); https://doi.org/10.1051/epjconf/202022501008.
9. G. BATTISTONI et al., "Overview of the FLUKA Code," *Ann. Nucl. Energy*, **82**, 10 (2015); https://doi.org/10.1016/j.anucene.2014.11.007.
10. S. U. DURAN, P. U. KICECI, and B. DEMIRKOZ, "Shield Design of the First Protective Collimator in the METU-Defocusing Beamline (DBL) Project," *Nucl. Technol.*, **208**, 364 (2021); https://doi.org/10.1080/00295450.2021.1888617.
11. U. ALVER et al., "Ulexite/HDPE-Bi_2O_3/HDPE Layered Composites for Neutron and Gamma Radiation Shielding," *Appl. Radiat. Isot.*, **200**, 110940 (2023); https://doi.org/10.1016/j.apradiso.2023.110940.
12. S. U. DURAN et al. "Radiation Shielding Properties of 5% HDPE/Boron Composites," *Rad. Conf. Proc*. **6**, 43 (2022); http://doi.org/10.21175/RadProc.2022.08.
13. V. VLACHOUDIS, "Flair: A Powerful But User Friendly Graphical Interface for FLUKA," *Proc. Int. Conf. Mathematics, Computational Methods and Reactor Physics*, Saratoga Springs, New York, May 3–7, 2009, Vol. 2, p. 790, American Nuclear Society (2009).
14. A. FERRARI et al., "FLUKA: A Multi-Particle Transport Code," CERN Yellow Report, CERN-2005-10 (2005); http://doi.org/10.2172/877507.
15. B. MUÇOGLLAVA, "A Novel Layered Boron-Based Neutron Shield Design and Results from Neutron and Gamma Irradiation Studies," Master's Thesis, Middle East Technical University (2022).
16. M. YIĞITOĞLU, "Radiation Environment Predictions for the IMECE Satellite and G4BEAMLINE Simulations for the METU-DBL Project," Master's Thesis, Middle East Technical University (2017).
17. M. M. GÜNTHER et al., "Dispersive Refraction of Different Light to Heavy Materials at MeV γ-Ray Energies," *Phys. Rev. A*, **97**, 063843 (2018); http://doi.org/10.1103/PhysRevA.97.063843.
18. C. ELLIOTT et al., "National Instruments LabVIEW: A Programming Environment for Laboratory Automation and Measurement," *J. Lab. Autom*., **12**, 17 (2007); http://doi.org/10.1016/j.jala.2006.07.012.